Inorg. Chem. **2004**, *43*, 1735–1742

Synthesis and Characterization of Bis(di-2-pyridylmethanamine)ruthenium(II)

Jin Chang, Susan Plummer, Elena S. F. Berman, Durwin Striplin, and David Blauch*

Department of Chemistry, Davidson College, Davidson, North Carolina 28035

Received July 28, 2003

The complex $Ru(dipa)_2^{2+}$ (dipa = di-2-pyridylmethanamine) has been prepared, yielding approximately a statistical ratio of the *meso* and *rac* isomers. The electronic spectra of both isomers show pyridyl $\pi \rightarrow \pi^*$ transitions in the UV region and MLCT bands in the visible region. The solvent dependence of the spectra provides evidence of hydrogen bond formation between the solvent and the NH_2 site on the ligand. The electrochemical properties of the two isomers are identical; each undergoes a reversible one-electron oxidation in acetonitrile ($E_{1/2}$ = 0.933 V vs Ag/AgCl) and in aqueous solution below pH 3 ($E_{1/2}$ = 0.786 V vs Ag/AgCl). In aqueous solution above pH 3, one-electron oxidation of the ruthenium center is followed by deprotonation of the ligand NH_2 site yielding a reactive amidoruthenium(III) species. The ruthenium-bound dipa ligand possesses structural constraints that prevent the usual oxidative dehydrogenation reaction, which would yield exclusively the corresponding imine. Instead the amidoruthenium(III) intermediate finds alternative reaction routes leading to multiple products.

Introduction

Oxidative transformations of ruthenium-bound amines have been the subject of several studies, with the catalytic role of the metal center being of special interest. In almost all cases, oxidation of an amineruthenium(II) complex leads to dehydrogenation of the ligand, yielding a coordinated imine.[1−3] For some primary amines, further oxidation of the imine to a nitrile is also possible.[2a] The utilization of ruthenium complexes as catalysts for the synthesis of imines and nitriles has also been described.[4]

The propensity of (amine)ruthenium(II) complexes to undergo oxidative dehydrogenation led us to ponder how such complexes might behave if this reaction route were blocked. Conversion of the amine to an imine requires both loss of a hydrogen and a change in bonding geometry from tetrahedral to planar at both the nitrogen and adjacent carbon. If any of these requirements cannot be satisfied, oxidative dehydrogenation should not be possible. If oxidative dehydrogenation cannot occur, how will (amine)ruthenium(II) complexes behave upon oxidation?

A comparison of the reactivities of Ru(II) complexes of 1,2-ethanediamine and 2,3-dimethyl-2,3-butanediamine provides an intriguing example of the effect of blocking the preferred oxidative dehydrogenation pathway. Ruthenium(II) complexes of 1,2-ethanediamine are irreversibly oxidized to the corresponding diimine.[1b] By contrast, the oxidation of ruthenium(II)-bound 2,3-dimethyl-2,3-butanediamine results in cleavage of the central carbon−carbon bond and imine formation to yield two $NH{=}C(CH_3)_2$ ligands.[5]

To explore this behavior, we have prepared Ru(II) complexes of di-2-pyridylmethanamine (dipa). Tridentate coordination of dipa forces the central carbon to maintain a tetrahedral geometry, thereby preventing formation of di-2-pyridylmethanimine (dipi). This report describes the synthesis and characterization of the two isomers (*meso* and *rac*) of the $Ru(dipa)_2^{2+}$ complex (Figure 1).

Experimental Section

Materials. $Ru(DMSO)_4Cl_2$ was prepared by published procedures.[6] Di-2-pyridyl ketone was obtained from Aldrich. Water was

* To whom correspondence should be addressed. E-mail: dablauch@davidson.edu.

(1) (a) Lane, B. C.; Lester, J. E. Basolo, F. *J. Chem. Soc., Chem. Commun.* **1971**, 1618−1619. (b) Mahoney, D. F.; Beattie, J. K. *Inorg. Chem.* **1973**, *12*, 2561−2565. (c) Alvarez, V. E.; Allen, R. J.; Matsubara, T.; Ford, P. C. *J. Am. Chem. Soc.* **1974**, *96*, 7686−7692. (d) Diamond, S. E.; Tom, G. M.; Taube, H. *J. Am. Chem. Soc.* **1975**, *97*, 2661−2664.

(2) (a) Keene, F. R.; Salmon, D. J.; Meyer, T. J. *J. Am. Chem. Soc.* **1976**, *98*, 1884−1889. (b) Brown, G. M.; Weaver, T. R.; Keene, F. R.; Meyer, T. J. *Inorg. Chem.* **1976**, *15*, 190−196. (c) Whebell, G. W.; Keene, F. R. *Aust. J. Chem.* **1986**, *39*, 2027−2035.

(3) (a) Yamaguchi, M.; Yamagishi, T. *Inorg. Chem.* **1993**, *32*, 2981−2982. (b) Yamaguchi, M.; Machiguchi, K.; Mori, T.; Kikuchi, K.; Ikemoto, I.; Yamagishi, T. *Inorg. Chem.* **1996**, *35*, 143−148.

(4) (a) Murahashi, S.-I.; Naota, T.; Hiroshi, T. *J. Chem. Soc., Chem. Commun.* **1985**, 613−614. (b) Bailey, A. J.; James, B. R. *Chem. Commun.* **1996**, 2343−2344.

(5) Wong, K.-Y.; Che, C.-M.; Li, C.-K.; Chiu, W.-H.; Zhou, Z.-Y.; Mak, T. C. W. *J. Chem. Soc., Chem. Commun.* **1992**, 754−6.

10.1021/ic030242a CCC: $27.50
Published on Web 02/03/2004

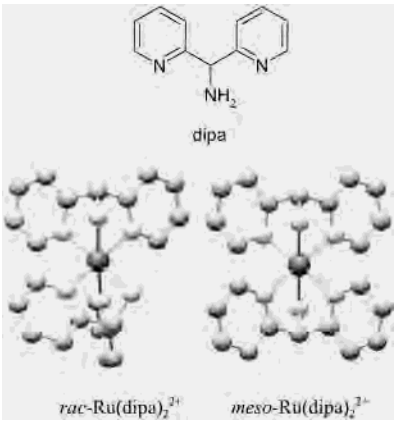

Figure 1. Structures of the dipa ligand and the two isomeric forms of the $Ru(dipa)_2^{2+}$ complex.

distilled and deionized prior to use; all other solvents and reagents were of analytical reagent grade and were used without additional purification. Elemental analyses were performed by Oneida Research Services, Inc.

Di-2-pyridyl Ketone Oxime. The procedure was a modification of that described by Blicke and Maxwell.[7] Di-2-pyridyl ketone (24.8 g, 0.135 mol) and hydroxylamine hydrochloride (13.0 g, 0.202 mol) were dissolved in 36 mL of ethanol. Sodium hydroxide (26.7 g, 0.666 mol) was slowly added to the solution with stirring over a period of 90 min, during which time the solution turned dark orange and a white precipitate formed. The solution was heated at reflux for 10 min and cooled to room temperature. The reaction mixture was treated with water (100 mL) and concentrated HCl (50 mL), and the ethanol was removed by rotary evaporation to yield a dark red solution. The product was precipitated by addition of saturated aqueous sodium carbonate (100 mL), isolated by vacuum filtration, washed with water, and dried in vacuo at room temperature to yield 29.4 g of hydrated product. ^{1}H NMR (300 MHz, $CDCl_3$, 298 K, TMS): δ 16.2 (br s, 1H, OH), 8.65 (d, J = 5.4 Hz, 1H, H6 of pyridine), 8.63 (d, J = 5.4 Hz, 1H, H6 of pyridine), 7.89 (dd, J = 7.9 and 1.6 Hz, 1H, H3 of pyridine), 7.83 (m, 2H, H4 of pyridine), 7.65 (d, J = 8.1 Hz, 1H, H3 of pyridine), 7.45 (td, J = 6.1 and 1.7 Hz, 1H, H5 of pyridine), 7.35 (td, J = 5.5 and 2.5 Hz, 1H, H5 of pyridine).

Di-2-pyridylmethanamine (dipa). The procedure was a modification of that described by Niemers.[8] Di-2-pyridyl ketone oxime (13.4 g, 60.6 mmol), ammonium acetate (20.2 g, 131 mmol), concentrated aqueous ammonia (180 mL, 3.1 mol), ethanol (120 mL), and water (120 mL) were combined in a 1 L flask. The solution was heated at reflux, and zinc powder (16.9 g, 258 mmol) was added over a period of 2 h, during which time gas was evolved and the reaction solution became dark red in color. Heating was continued for 3 h, during which time the solution turned orange and a white solid formed. The solid was removed by vacuum filtration, and the ethanol was removed from the filtrate by rotary evaporation. Sodium hydroxide (42.8 g, 1.07 mol) was added to the solution, initially producing a white solid which redissolved as the remainder of the sodium hydroxide was added. The dark red solution was extracted with five 50 mL portions of ether. The ether was removed from the combined extracts by rotary evaporation, and the residue was purified by vacuum distillation (146−154 °C at 5 Torr) to yield 7.02 g (63%) of a light yellow oil. ^{1}H NMR (300 MHz, $CDCl_3$, 298 K, TMS): δ 8.52 (d, J = 4.5 Hz, 2H, H6 of pyridine), 7.57 (td, J = 7.7 and 1.5 Hz, 2H, H4 of pyridine), 7.38 (d, J = 7.8 Hz, 2H, H3 of pyridine), 7.08 (td, J = 6.0 and 1.8 Hz, 2H, H5 of pyridine), 5.32 (s, 1H, C*H*NH_2), 2.54 (br s, 2H, CHN*H*$_2$).

[Ru(dipa)$_2$](PF$_6$)$_2$. $Ru(DMSO)_4Cl_2$ (7.13 g, 14.7 mmol), water (100 mL), and ethanol (250 mL) were placed in a 1-L flask, and the solution was purged with nitrogen gas. A nitrogen-purged solution of di-2-pyridylmethanamine (5.76 g, 31.3 mmol) in ethanol (10 mL) was added to the flask. An additional 140 mL of nitrogen-purged ethanol was added to the flask, and the solution was heated at reflux under a nitrogen atmosphere. The progress of the reaction was monitored by periodically drawing small aliquots of the reaction solution, diluting the aliquot in water, and recording the UV−vis spectrum. After 86 h the UV−vis spectrum of the reaction solution ceased to change. A saturated aqueous solution of ammonium hexafluorophosphate was added to the hot reaction solution, which was then cooled in a refrigerator overnight. The solid was isolated by vacuum filtration and dried in vacuo at room temperature, yielding 10.3 g (92%) of crude $[Ru(dipa)_2](PF_6)_2$. The *meso* and *racemic* isomers of the complex were separated by repeated recrystallizations from ethanol and ethanol−water mixtures. The hexafluorophosphate salt of the *meso* complex has a very low solubility in ethanol whereas that of the *racemic* isomer is moderately soluble. The final yields of purified *meso*-$[Ru(dipa)_2](PF_6)_2$ and *rac*-$[Ru(dipa)_2](PF_6)_2$ were 1.92 and 6.07 g, respectively, which correspond with 17% and 54% of the total theoretical yield.

***meso*-[Ru(dipa)$_2$](PF$_6$)$_2$.** Anal. Calcd for $C_{22}H_{22}F_{12}N_6P_2Ru$: C, 34.70; H, 2.91; N, 11.04. Found: C, 34.82; H, 2.72; N, 10.67. ^{1}H NMR (300 MHz, acetone-d_6, 298 K, TMS): δ 8.96 (d, J = 5.5 Hz, 2H, H6 of pyridine), 8.16 (d, J = 7.4 Hz, 2H, H3 of pyridine), 8.09 (dd, J = 7.4 and 7.6 Hz, 2H, H4 of pyridine), 7.45 (dd, J = 5.4 and 7.6 Hz, 2H, H5 of pyridine), 6.45 (s, 1H, C*H*NH_2), 5.10 (s, 2H, CHN*H*$_2$).

***rac*-[Ru(dipa)$_2$](PF$_6$)$_2$.** Anal. Calcd for $C_{22}H_{22}F_{12}N_6P_2Ru$: C, 34.70; H, 2.91; N, 11.04. Found: C, 34.68; H, 2.52; N, 10.77. ^{1}H NMR (300 MHz, acetone-d_6, 298 K, TMS): δ 8.69 (d, J = 5.5 Hz, 1H, H6 of pyridine), 8.53 (d, J = 5.4 Hz, 1H, H6 of pyridine′), 8.17 (d, J = 7.8 Hz, 1H, H3 of pyridine), 8.14 (d, J = 7.8 Hz, 1H, H3 of pyridine′), 8.11 (dd, 7.6 and 7.8 Hz, 1H, H4 of pyridine), 8.04 (dd, J = 7.6 and 7.8 Hz, 1H, H4 of pyridine′), 7.54 (dd, J = 5.5 and 7.6 Hz, 1H, H5 of pyridine), 7.43 (dd, J = 5.4 and 7.6 Hz, 1H, H5 of pyridine′), 6.51 (s, 1H, C*H*NHH), 5.49 (d, J = 9.8 Hz, 1H, CHN*H*H), 5.25 (d, J = 9.8 Hz, 1H, CHNH*H*).

***rac*-[Ru(dipa)$_2$]Cl$_2$·H$_2$O.** *rac*-$[Ru(dipa)_2](PF_6)_2$ (4.17 g, 5.48 mmol) dissolved in 100 mL of acetone was added to a solution of tetrabutylammonium chloride (15.3 g, 55.1 mmol) in 75 mL of acetone, resulting in immediate formation of a yellow precipitate. The mixture was stirred for 1 h, at which time the yellow precipitate was isolated by vacuum filtration and washed with acetone. The solid was dissolved in absolute ethanol and reprecipitated by slow addition of acetone to the hot ethanol solution. After cooling in a freezer, the yellow solid was isolated by vacuum filtration and dried in vacuo at room temperature yielding 2.38 g (80%) of product. Anal. Calcd for $C_{22}H_{24}Cl_2N_6ORu$: C, 47.15; H, 4.32; N, 14.99. Found: C, 47.05; H, 4.70; N, 14.76.

Chemical Oxidation of *rac*-[Ru(dipa)$_2$](PF$_6$)$_2$. Chemical oxidations were performed with bromine or potassium persulfate. In a typical reaction, *rac*-$[Ru(dipa)_2](PF_6)_2$ (0.40 g, 0.53 mmol) was partially dissolved in 100 mL of water containing sodium acetate (0.82 g, 10. mmol). The yellow solution was treated with the oxidant, bromine (0.4 mL, 15 mmol) or potassium persulfate (2.91

(6) (a) Evans, P.; Spencer, A.; Wilkinson, G. *J. Chem. Soc., Dalton Trans.* **1973**, 204−209. (b) Szafran, Z.; Pike, R. M.; Singh, M. M. *Microscale Inorganic Chemistry*; Wiley: New York, 1991.
(7) Blicke, F. F.; Maxwell, C. E. *J. Am. Chem. Soc.* **1939**, *61*, 1780−2.
(8) Niemers, E. *Synthesis* **1976**, 593−5.

g, 18 mmol) dissolved in 80 mL water, yielding a dark purple solution containing a fine dark precipitate. After being stirred for up to 2 h, the solution was heated to dissolve the solid. Saturated aqueous ammonium hexafluorophosphate was added, and the solution was allowed to cool overnight in a refrigerator. The dark purple solid was isolated by vacuum filtration and allowed to air-dry. Yields ranged from 0.19 to 0.23 g. In each case, TLC analysis of the product showed it to contain multiple components.

Spectroscopy. ^{1}H, COSY, and *J*-resolved NMR spectroscopic measurements were performed on a Bruker AC-300 spectrometer (300 MHz). Chemical shifts are reported in ppm and referenced to TMS. UV−vis measurements were performed on an HP 8453 spectrometer or a Cary 300 Bio spectrometer. IR spectroscopy was performed using a Midac 1700-Series instrument with samples of the hexafluorophosphate salts of the complexes suspended in KBr pellets. The free dipa ligand was deposited on salt plates for IR measurements. MALDI-TOF mass spectroscopy measurements were performed on a PerSeptive Biosystems Voyager DE Bio-Spectrometry workstation. Samples were prepared by depositing a layer of α-cyano-4-hydroxycinnamic acid (CHCA) matrix from a saturated solution in CH_2Cl_2/methanol and then applying a drop of a solution of the analyte dissolved in methanol. Laser desorption was performed at 337 nm, and the TOF mass spectrometer operated with a 20 kV accelerating potential. Irganox 1010 was added as a reference material, and calibration was accomplished using ion peaks associated with the Irganox 1010 and the CHCA matrix.

Electrochemistry. Cyclic voltammetry was performed with a PAR 273A potentiostat using a single-compartment cell equipped with a platinum counter electrode. All solutions were purged with nitrogen prior to analysis. Measurements in aqueous solution employed a glassy carbon disk working electrode (0.0707 cm^2) and an Ag/AgCl reference electrode. Measurements in acetonitrile (containing 0.10 M tetrabutylammonium perchlorate as supporting electrolyte) employed a platinum disk working electrode (0.0177 cm^2) and a ferrocene/ferrocenium reference electrode, which was calibrated immediately before and after each use. All potentials are reported vs aqueous Ag/AgCl.

Computations. Density functional theory (DFT) computations employing Becke's three-parameter hybrid functional[9] using the Lee, Yang, and Parr correlation function[10] (b3lyp) were performed using the Gaussian 98 software package (revision A.7).[11] The lanl2dz basis set was employed in all computations. This basis set uses the Hay−Wadt (Los Alamos) effective core potentials[12] for ruthenium and the Dunning−Hay double-ζ (D95) basis set[13] for hydrogen, carbon, oxygen, and nitrogen. Frequency calculations were performed on each optimized geometry to ensure the geometry corresponded with an energy minimum (no imaginary frequencies) and to determine the thermodynamic properties of the complex. Energies for electronic transitions were computed using the single-excitation configuration interaction (CIS) method.[14]

Results and Discussion

Synthesis. The ruthenium(II) complexes of di-2-pyridylmethanamine were prepared by direct reaction of the free ligand with $Ru(DMSO)_4Cl_2$ in an ethanol−water mixture under nitrogen, and the progress of the reaction was followed by UV−vis spectroscopy. The $Ru(dipa)_2^{2+}$ complex can exist as two different isomers: the centrosymmetric *meso* and the dissymmetric *rac* isomers, in which the NH_2 groups for the two dipa ligands are oriented trans and cis, respectively. During the purification of the $Ru(dipa)_2(PF_6)_2$ product, it was observed that the majority of the product was appreciably soluble in hot ethanol while a portion of the product remained undissolved. This difference in solubilities was exploited to separate the sample into two pure compounds, which were found to be the *rac* and *meso* isomers. The higher solubility in ethanol and ethanol−water mixtures of the *rac* isomer compared with that of the *meso* isomer is consistent with the difference in dipole moments (1.69 and 0 D, respectively, on the basis of gas-phase DFT computations). The hexafluorophosphate salts of both isomers show a low solubility in water (several hundred micromolar). For some measurements involving the *rac* isomer, we employed the more soluble chloride salt.

The isomers were identified by NMR spectroscopy (Figure 2). The four pyridyl groups in the *meso* complex are in equivalent environments, leading to a relatively simple NMR spectrum containing peaks for the four different pyridyl protons and singlets for the NH_2 and methine protons. The two pyridyl groups of a dipa ligand are not equivalent in the *rac* complex, owing to the lower symmetry of this isomer, and consequently, two sets of signals for the pyridyl protons appear in the NMR spectrum. The two NH_2 protons are also in nonequivalent environments, giving rise to a pair of doublets.

The UV−vis absorbance spectra of *meso*- and *rac*-$Ru(dipa)_2(PF_6)_2$ in water are shown in Figure 3. Fitting the absorbance spectrum of the final reaction solution with a linear combination of the spectra of the *rac* and *meso* complexes shows the distribution of isomers to be 72%:28% *rac*:*meso*. This product distribution is close to the 76%:24% distribution of isolated purified products, though this yield ratio is less reliable owing to loss of material during the repeated recrystallizations.

The preparation of bis(di-2-pyridylmethanamine) complexes of a series of first-row transition metals has been reported.[15] Exclusively *rac* isomer was obtained for the Fe(II), Fe(III), and Co(III) complexes whereas exclusively *meso*

(9) (a) Becke, A. D. *Phys. Rev., Ser. A* **1988**, *38*, 3098−3100. (b) Becke, A. D. *J. Chem. Phys.* **1993**, *98*, 1372−1377. (c) Becke, A. D. *J. Chem. Phys.* **1993**, *98*, 5648−5652. (d) Stevens, P. J.; Devlin, F. J.; Chablowski, C. F.; Frisch, M. J. *J. Phys. Chem.* **1994**, *98*, 11623.
(10) Lee, C.; Yang, W.; Parr, R. G. *Phys. Rev.* **1988**, *B37*, 785−789.
(11) Frisch, M. J.; Trucks, G. W.; Schlegel, H. B.; Scuseria, G. E.; Robb, M. A.; Cheeseman, J. R.; Zakrzewski, V. G.; Montgomery, J. A., Jr.; Stratmann, R. E.; Burant, J. C.; Dapprich, S.; Millam, J. M.; Daniels, A. D.; Kudin, K. N.; Strain, M. C.; Farkas, O.; Tomasi, J.; Barone, V.; Cossi, M.; Cammi, R.; Mennucci, B.; Pomelli, C.; Adamo, C.; Clifford, S.; Ochterski, J.; Petersson, G. A.; Ayala, P. Y.; Cui, Q.; Morokuma, K.; Malick, D. K.; Rabuck, A. D.; Raghavachari, K.; Foresman, J. B.; Cioslowski, J.; Ortiz, J. V.; Baboul, A. G.; Stefanov, B. B.; Liu, G.; Liashenko, A.; Piskorz, P.; Komaromi, I.; Gomperts, R.; Martin, R. L.; Fox, D. J.; Keith, T.; Al-Laham, M. A.; Peng, C. Y.; Nanayakkara, A.; Gonzalez, C.; Challacombe, M.; Gill, P. M. W.; Johnson, B.; Chen, W.; Wong, M. W.; Andres, J. L.; Gonzalez, C.; Head-Gordon, M.; Replogle, E. S.; Pople, J. A. *Gaussian 98*, revision A.7; Gaussian, Inc.: Pittsburgh, PA, 1998.
(12) (a) Hay, P. J.; Wadt, W. R. *J. Chem. Phys.* **1985**, *82*, 270−283. (b) Wadt, W. R.; Hay, P. J. *J. Chem. Phys.* **1985**, *82*, 284−298. (c) Hay, P. J.; Wadt, W. R. *J. Chem. Phys.* **1985**, *82*, 299−310.
(13) Hunning, T. H., Jr.; Hay, P. J. In *Modern Theoretical Chemistry*; Schaefer, H. F., III, Ed.; Plenum: New York, 1976; pp 1−28.
(14) Foresman, J. B.; Head-Gordon, M.; Pople, J. A.; Frisch, M. J. *J. Phys. Chem.* **1992**, *96*, 135.
(15) Bernhardt, P. V.; Comba, P.; Mahu-Rickenbach, A.; Stebler, S.; Steiner, S.; Várnagy, K.; Zehnder, M. *Inorg. Chem.* **1992**, *31*, 4194−4200.

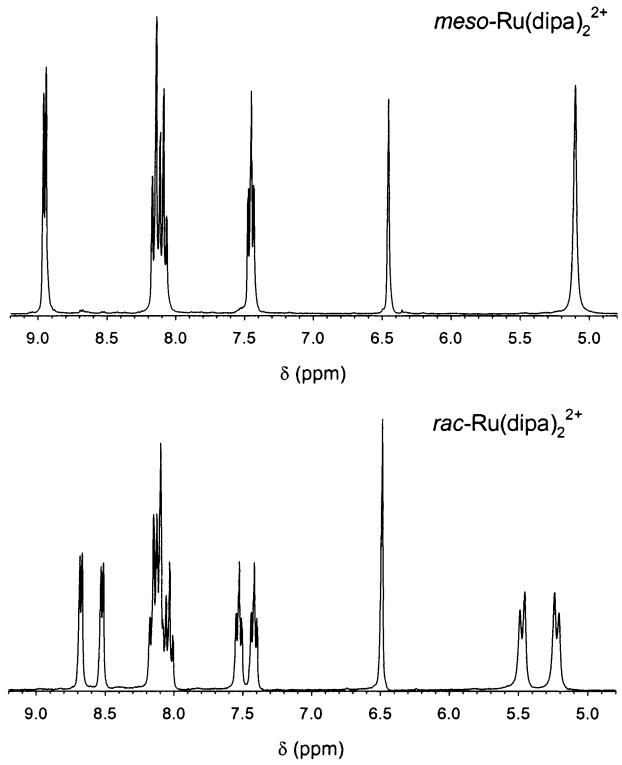

Figure 2. ^{1}H NMR spectra of *meso*-Ru(dipa)$_2$(PF$_6$)$_2$ and *rac*-Ru(dipa)$_2$-(PF$_6$)$_2$ in acetone-d_6.

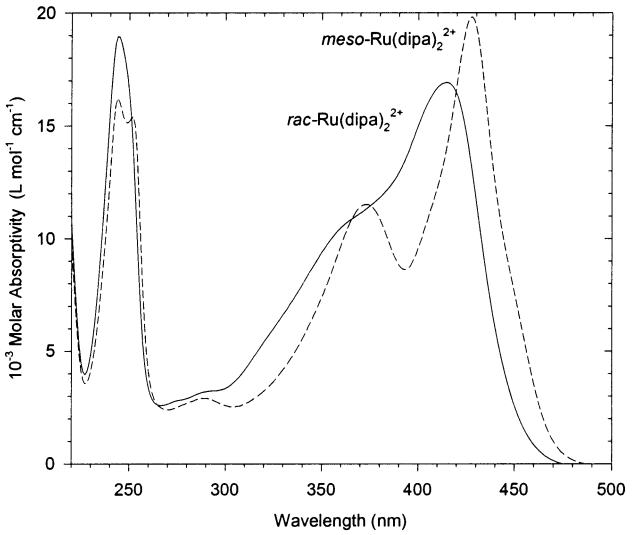

Figure 3. UV−vis absorbance spectra for *meso*-Ru(dipa)$_2$(PF$_6$)$_2$ (dashed line) and *rac*-Ru(dipa)$_2$(PF$_6$)$_2$ (solid line) in water.

isomer was obtained for the Ni(II) and Cu(II) complexes. Those authors attribute the shift from *rac* to *meso* to the increasing size of the metal ion, which decreases steric crowding of the two dipa ligands arising from steric repulsions between an NH proton on one ligand and a 6-pyridyl proton on the other ligand.

The DFT-optimized geometries for *meso*-Fe(dipa)$_2^{2+}$ and *meso*-Ru(dipa)$_2^{2+}$ show this NH···HC distance to be 2.25 and 2.48 Å, respectively.[16] These values are close to twice the van der Waals radius of hydrogen (1.20 Å),[17] suggesting that steric crowding of these hydrogens is modest. At 100 °C the DFT computations predict $\Delta G° = -10.39$ kJ mol^{-1} and -7.97 kJ mol^{-1} for the gas-phase *meso*-to-*rac* isomerization for Fe(dipa)$_2^{2+}$ and Ru(dipa)$_2^{2+}$, corresponding with yield distributions of the *rac* isomer of 98% and 96%, respectively. The similarity of the thermodynamic data for the Fe(II) and Ru(II) complexes suggests that thermodynamic control of the Ru(dipa)$_2^{2+}$ product distribution would produce exclusively the *rac* isomer, as was reported for Fe(dipa)$_2^{2+}$. The experimental product distribution for Ru(dipa)$_2^{2+}$ is most likely a consequence of kinetic control with only slight progress toward equilibration. This behavior is not surprising given the much lower ligand lability for second- and third-row transition-metal complexes.

Spectroscopy and Electronic Structure. The molecular orbital diagrams for the gas-phase *meso*-Ru(dipa)$_2^{2+}$ (C_{2h} symmetry) and *rac*-Ru(dipa)$_2^{2+}$ (C_2 symmetry) were determined by density functional theory (b3lyp) using an effective core potential basis set (lanl2dz).[18] For each complex, the three highest occupied orbitals are predominantly ruthenium d orbitals with modest delocalization onto the pyridyl rings. A manifold of four ligand-based π bonding orbitals lie just below the occupied Ru d orbitals. The dominant character of the eight lowest unoccupied molecular orbitals is ligand-centered π*, though most of these orbitals also display some degree of Ru d character. The lower symmetry of the *rac* complex leads to greater mixing of Ru d and pyridine π* than is the case for the *meso* isomer. At still higher energies one finds σ* orbitals for the Ru−NH$_2$ and Ru−pyridyl interactions. (Energy diagrams and isosurfaces appear in the Supporting Information.)

The UV−vis spectra of the complexes in water (Figure 3 and Table 1) display strong UV bands and a broad set of bands at the edge of the visible region (Table 1). The origin of these transitions were assigned on the basis of single-excitation configuration interaction (CIS) calculations. These computations indicate that the observed UV bands arise from excitation of an electron from a pyridyl π orbital (py$_3$) to the LUMO (pyridyl π*) orbital. The transitions at the edge of the visible region are associated with metal-to-ligand charge transfer (MLCT) from the three highest occupied orbitals (Ru d) to the six lowest lying unoccupied orbitals (pyridyl π*). This behavior, typical of pyridylruthenium(II) complexes, is observed for the *cis*-Ru(bpy)$_2$(NH$_3$)$_2^{2+}$ complex (Table 1).[19]

Experimental evidence for the assignment of the MLCT and pyridine-based $\pi \rightarrow \pi$* transitions is found in the solvent dependence of the UV−vis spectra. The wavelengths of the

(16) Crystallographic data for *rac*-[Fe(dipa)$_2$](ClO$_4$)$_2$·2H$_2$O from ref 15 provides Fe−N bond lengths of 2.00 and 1.95 Å for the NH$_2$ and pyridyl sites, respectively. Our DFT computations gave distances of 2.07 and 2.01 Å, respectively.

(17) Rodger, G. E. *Descriptive Inorganic Coordination, and Solid-State Chemistry*, 2nd ed.; Brooks/Cole: Toronto, 2002; p 167.

(18) We were unable to obtain X-ray crystallographic data for the Ru-(dipa)$_2^{2+}$ complexes, but the structurally similar *trans*-Ru(bpy)$_2$-(NH$_3$)$_2^{2+}$ complex (bpy = 2,2′-bipyridine) has been found to have an Ru−N bond lengths (in Å) of 2.11 for the amine site and 2.06 for the bpy sites. (Cordes, A. W.; Durham, B. Pennington, W. T.; Kuntz, B.; Allen, L. *J. Crystallogr. Spectrosc. Res.* **1992**, *22*, 699−704.) The optimized DFT geometry for the *meso*-Ru(dipa)$_2^{2+}$ complex provides Ru−N bond lengths of 2.17 (NH$_2$) and 2.11 (pyridyl).

(19) Assefa, Z.; Stanbury, D. M. *J. Am. Chem. Soc.* **1997**, *119*, 521−530.

Table 1. Spectroscopic Properties of $Ru(dipa)_2^{2+}$ Complexes

	meso-$Ru(dipa)_2^{2+}$		*rac*-$Ru(dipa)_2^{2+}$	*cis*-$Ru(bpy)_2(NH_3)_2^{2+}$ [a]
		λ_{max}/nm ($\epsilon_{max}/10^3\ M^{-1}\ cm^{-1}$)[b]		
	244 (16.2)	252 (15.4)	244 (19.0)	292
	373 (11.5)	428 (19.8)	415 (16.9)	346
				486
		Kamlet−Taft Parameters[c]		
ν_o ($10^3\ cm^{-1}$)	27.44 ± 0.06	24.18 ± 0.06	24.80 ± 0.06	
p (cm^{-1})	−590 ± 60	−650 ± 60	−580 ± 60	
b (cm^{-1})	−1020 ± 60	−1090 ± 60	−1100 ± 40	
a (cm^{-1})	163 ± 26	87 ± 26	122 ± 24	
		Gutmann Acceptor−Donor Relation[d]		
slope	−0.123 ± 0.007	−0.116 ± 0.012	−0.116 ± 0.013	−0.127
intercept ($10^3\ cm^{-1}$)	24.00 ± 0.05	27.30 ± 0.10	24.62 ± 0.10	20.86

[a] Reference 19. [b] Absorbance maxima in aqueous solution. Assignments given in main text. The *meso* isomer show two sets of peaks. [c] Coefficients *a* and *b* characterize the solute's ability to accept and donate a hydrogen bond, and *p* characterizes dipole effects. All points are accurately predicted within the experimental error of ±1 nm. [d] Water, which lies off the trend line, was not included in the regression. To permit comparison with results for the other complexes, values for *meso*-$Ru(dipa)_2^{2+}$ do not include data in 1,2-dichloroethane.

UV transitions are essentially independent of the solvent, varying by only 2 nm over the range of solvents employed in the study, consistent with a ligand-based transition. The peak positions in the visible portion of the spectrum display a strong solvent dependence. This solvatochromatic effect was analyzed by fitting the frequency of the optical transition to a linear combination of the Kamlet−Taft α, β, and π^* parameters (Table 1).[20] The dominant influences of the solvent arise from polarity effects (*p*) and the ability of the solvent to accept a hydrogen bond from the complex (*b*). The polarity effect is consistent with an MLCT, which produces an excited-state whose dipole moment differs from that of the ground state. The hydrogen bonding effect arises from donation of a hydrogen bond from the coordinated amine to the solvent. Amines in general are hydrogen bond donors, and coordination of the amine to the Ru(II) center withdraws electron density from the amine nitrogen making the amine a better hydrogen bond donor. The nonzero value of the coefficient *a* indicates the complex has some ability (at least phenomenologically) to accept a hydrogen bond from the solvent, but this behavior plays only a small role in the solvation process. It is not obvious where this interaction might occur, though it may involve solvent interactions with the π orbitals on the pyridyl groups. In any event, this contribution is very small, and reasonable fits of the experimental data may be obtained using only a three-parameter (ν_o, *p*, and *b*) model.

An alternative method for evaluating the role of donor−acceptor interactions on the spectra is to correlate the energy of the transition with the Gutmann donor number (DN), as illustrated in Figure 4.[21] The behavior corresponds closely with that reported for the structurally similar $Ru(bpy)_2(NH_3)_2^{2+}$ complex (Table 1).[22] The authors in that study also concluded that the solvent forms a hydrogen bond with the coordinated NH_3, resulting in an increase in electron density at the metal.

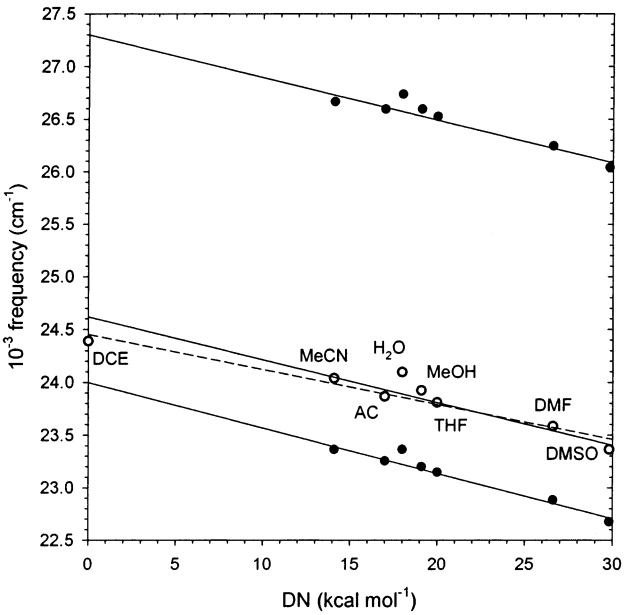

Figure 4. Variation of frequency of the electronic transition (visible region) with the solvent donor number for *rac*-$Ru(dipa)_2^{2+}$ (open circles) and *meso*-$Ru(dipa)_2^{2+}$ (solid circles, two electronic transitions). The solvents are 1,2-dichloroethane (DCE), acetonitrile (MeCN), acetone (AC), water, methanol (MeOH), tetrahydrofuran (THF), *N*,*N*-dimethylformamide (DMF), and dimethyl sulfoxide (DMSO). Lines-of-best-fit (solid lines) do not include data for DCE or water. The dashed line includes the DCE point.

The effect of this hydrogen bonding between the solvent and the Ru−NH_2 site on the MLCT transition must be an indirect, inductive effect, because neither orbital involved in the MLCT has significant electron density at the NH_2 site (see the above discussion). This hydrogen-bonding interaction was modeled computationally by explicitly placing water molecules on each NH_2 to established the proposed hydrogen-bonding interaction. Computations were performed with one water molecule associated with each amine hydrogen in the complex. As expected, the introduction of the water molecules does not shift the wavelength of the $\pi \rightarrow \pi^*$ transition whereas the computed wavelength of the MLCT transition experiences a substantial shift upon addition of the water. For the *meso* complex, the frequency shifts of the three dominant transitions are −1410, −1670, and −2450 cm^{-1}, respectively. The direction of this shift is consistent with

(20) Kamlet, M. J.; Abboud, J.-L.; Abraham, M. H.; Taft, R. W. *J. Org. Chem.* **1983**, *48*, 2877−2887.
(21) (a) Gutmann, V. *The Donor−Acceptor Approach to Molecular Interactions*; Plenum Press: New York, 1978. (b) Gutmann, V. *Coord. Chem. Rev.* **1976**, *18*, 225−255.
(22) Curtis, J. C.; Sullivan, B. P.; Meyer, T. J. *Inorg. Chem.* **1983**, *22*, 224−236.

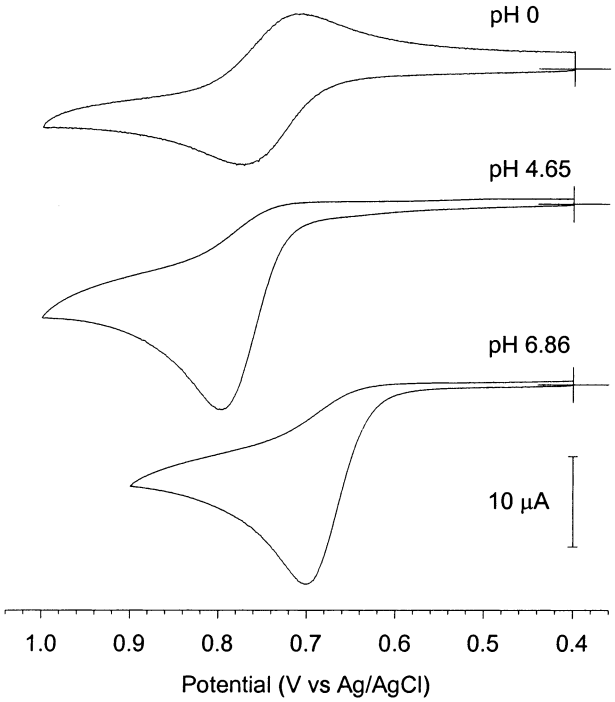

Figure 5. Cyclic voltammograms (50 mV s^{-1}) of 1.04 mM aqueous *rac*-Ru(dipa)$_2^{2+}$ solutions at various pH: 1.0 M H_2SO_4 (pH 0, top); CH_3COOH/CH_3COONa ($\mu = 0.10$ M, pH 4.65, middle); NaH_2PO_4/Na_2HPO_4 (pH 6.86, $\mu = 0.10$ M, bottom).

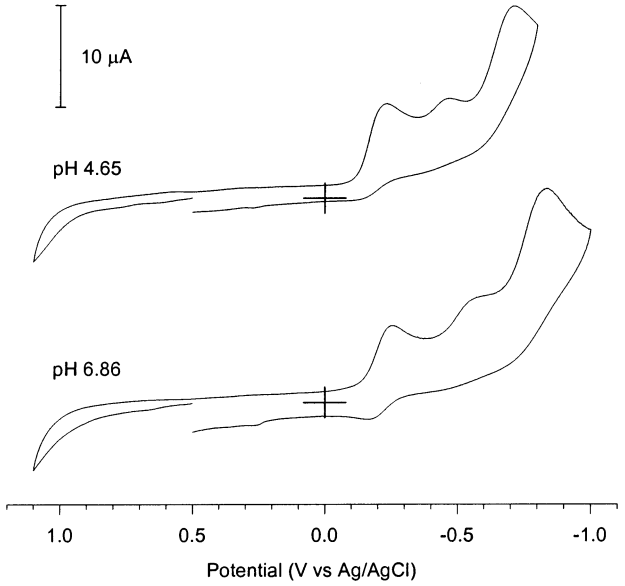

Figure 6. Cyclic voltammograms (100 mV s^{-1}) of 2.00 mM *rac*-Ru(dipa)$_2^{2+}$ in aqueous solution after controlled-potential electrolysis in CH_3COOH/CH_3COONa (pH 4.65, top) and NaH_2PO_4/Na_2HPO_4 (pH 6.86, bottom) at $E = +1.00$ V and $+0.90$ V, respectively.

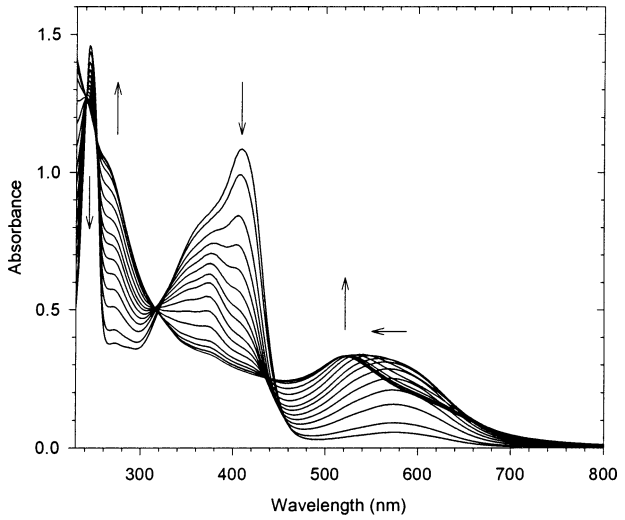

Figure 7. Oxidation of *rac*-Ru(dipa)$_2^{2+}$ (69 μM) by $S_2O_8^{2-}$ (1.8 mM) in aqueous NaH_2PO_4/Na_2HPO_4 (pH 6.86) at 25 °C. Spectra were recorded at 29, 43, 73, 103, 138, 183, 243, 303, 423, 603, 903, 1503, 2103, 3033, and 4413 s.

that observed experimentally in changing the solvent from a poor (e.g., DCE) to a good (e.g., H_2O) hydrogen bond acceptor. Similar behavior is observed for the *rac* complex, where the most intense band shows $\Delta\nu = -1930$ cm^{-1}. The inclusion of the four water molecules does not change the nature of the orbitals involved in the metal-to-ligand transfer, and none of these orbitals place electron density onto the water (or NH_2 sites). The hydrogen-bonding interaction at the amine site transfers electron density to the metal center, decreasing the Mulliken charge on the ruthenium from 0.80 to 0.75 (*meso*) and 0.84 to 0.78 (*rac*). The energies of all the orbitals are increased, with the effect being greatest for the Ru d orbitals (ca.1.1 eV) and slightly less for the pyridyl π^* orbitals (ca. 0.85 eV), as one would expect.

Electrochemistry. The electrochemical behavior of *meso*-Ru(dipa)$_2^{2+}$ and *rac*-Ru(dipa)$_2^{2+}$ are identical within experimental error. Cyclic voltammograms obtained in acetonitrile show a reversible one-electron oxidation of the complex with $E_{1/2} = 0.933$ ($\pm$0.015) V. This half-wave potential is similar to that of the Ru(bpy)$_2$(NH$_3$)$_2^{3+/2+}$ couple (0.960 V).[2b] In highly acidic aqueous solution (pH < 3), both the *meso*- and *rac*-Ru(dipa)$_2^{2+}$ complexes display a single one-electron reversible cyclic voltammetric wave with $E_{1/2} = 0.786$ ($\pm$0.006) V. In aqueous solutions above pH 3, the oxidation becomes irreversible with the voltammetric wave shifting to lower potentials as the pH increases (Figure 5). The accompanying increase in the anodic peak current indicates that the overall oxidation is a multielectron process; the initial one-electron oxidation of Ru(dipa)$_2^{2+}$ to Ru(dipa)$_2^{3+}$ is quickly followed by additional oxidation. Solutions of the *rac* complex were subjected to controlled-potential electrolysis in acetate and phosphate buffers at pH 4.65 and 6.86, respectively. During the course of the electrolysis the original yellow solution turned green and then ultimately a dark purple color. Cyclic voltammograms obtained from the resulting solutions show a series of irreversible reductions at negative potentials (Figure 6).

Oxidation of *rac*-Ru(dipa)$_2^{2+}$. The oxidation of *rac*-[Ru(dipa)$_2$]Cl$_2$ in aqueous phosphate buffer (pH 6.86) by potassium persulfate was followed spectrophotometrically (Figure 7). Spectra acquired at early times show an isosbestic point at 319 nm. As the reaction proceeds, that isosbestic point disappears while isosbestic points at 240, 250, 316, and 435 nm appear as the reaction reaches completion, indicating that there are more than two absorbing species in the reaction solution. The set of spectra were analyzed by principal component analysis (PCA) to determine the number of different absorbing species in the solution.[23] Various

methods (e.g., *F*-test, χ-square test) for distinguishing between those eigenvectors attributable to an absorbing species and those attributable to noise indicate that there are five or six absorbing species in the reaction solution. These findings taken together with the spectroscopic evidence described below indicate that *rac*-Ru(dipa)$_2^{2+}$ is oxidized to multiple products in a multistep mechanism.

The products of the oxidation of *rac*-Ru(dipa)$_2^{2+}$ were obtained by treating the complex with bromine or potassium persulfate in aqueous sodium acetate solutions and isolating the product by precipitation with aqueous ammonium hexafluorophosphate. The characteristics of the dark purple product obtained with the two different oxidants were very similar (but not identical). The ^{1}H NMR spectrum of the oxidized *rac*-Ru(dipa)$_2^{2+}$ reveals a proliferation of peaks in the aromatic region, indicating the presence of several nonequivalent pyridine rings. There is also an increase in the number of signals for the NH_2 and methine protons. Of particular note is the drastic decrease in intensities for the NH_2 and methine protons. In the original *rac*-Ru(dipa)$_2^{2+}$ complex, the ratio of integrals for pyridyl H:NH_2:methine H signals is 8:2:1. The ratios for the bromine and persulfate oxidized samples are 8:0.1:0.2 and 8:0.1:0.3, respectively. This loss of signal for the CH$-NH_2$ linkage indicates it is the site subject to oxidation. No new peaks were observed for the oxidized samples at chemical shifts below 5 ppm (or above 9.2 ppm). There is either no reaction at the pyridyl rings or any such reaction does not destroy the aromatic character of the rings. The distinction between pyridyl and CH$-NH_2$ signals was made on the basis of chemical shifts and COSY spectra, with methine protons showing no coupling and the nonequivalent NH_2 protons being coupled with each other. If the amine site were transformed into an imine or perhaps oxime functionality, the corresponding proton might be mistaken for a methine site. The ultimate conclusion, though, that the $CHNH_2$ branch of the ligand is the site of oxidation is unchanged.

Additional evidence for reaction at the aliphatic amine site is provided by IR spectroscopy. The asymmetric and symmetric N$-$H stretching frequencies occur at 3370 and 3289 cm^{-1}, respectively, in the free dipa ligand. Coordination of the dipa ligand to ruthenium(II) results in a shift of the asymmetric N$-$H stretching frequency to 3331 and 3344 cm^{-1} in the *meso* and *rac* complexes, respectively; there is no change in the frequency of the symmetric vibration upon coordination. This shift to lower frequency is attributable to weakening of the N$-$H bond upon coordination of the amine. (Interpretation of the IR data is complicated, however, because the vibrational frequencies are also influenced by interactions of the amine with the counterion and with water.[24]) Oxidation of the *rac*-[Ru(dipa)$_2$](PF$_6$)$_2$ complex results in almost complete elimination of the peaks for the two N$-$H stretching modes.

An attempt was made to purify a portion of the persulfate-oxidized material by column chromatography (Sephadex-SP C-25) with a mobile phase of aqueous HCl. Most of the material eluted as a long blue-purple running band with 0.5 M HCl. A small dark purple band remained on the column and could not be eluted by 6 M HCl. The inability to elute one of the components from Sephadex-SP C-25 with 6 M HCl indicates a highly charged binuclear (or higher) complex.

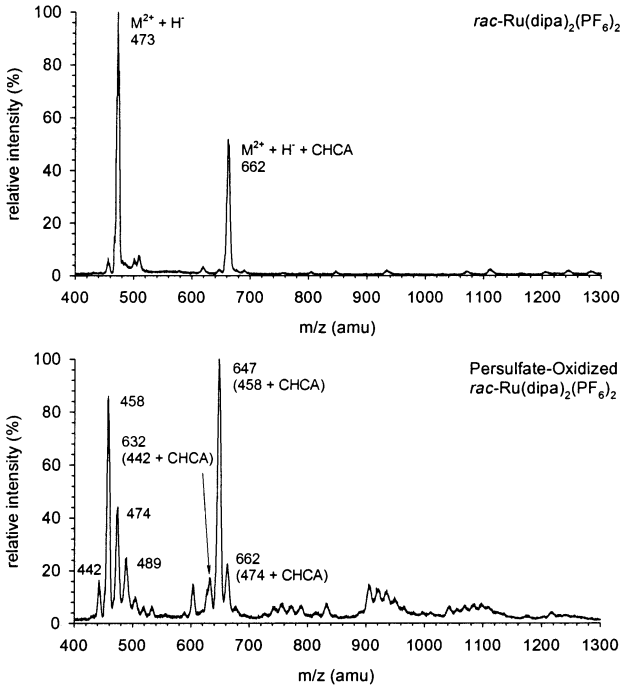

Figure 8. MALDI-TOF mass spectra of *rac*-Ru(dipa)$_2$(PF$_6$)$_2$ (top) and persulfate-oxidized *rac*-Ru(dipa)$_2$(PF$_6$)$_2$ in an α-cyano-4-hydroxycinnamic acid (CHCA) matrix.

The elemental analysis of the dark purple hexafluorophosphate salt of the persulfate-oxidized *rac*-Ru(dipa)$_2^{2+}$ (C, 34.65; H, 2.75; N, 10.68) was essentially identical with that of the bright yellow *rac*-[Ru(dipa)$_2$](PF$_6$)$_2$ (C, 34.68; H, 2.52; N, 10.77), indicating that oxidation of the complex produced a negligible change in structure or that multiple products exist with mass loss by one product offset by the gains of a different product. The limits of the precision of the elemental analysis data and the low atomic mass for hydrogen make it impossible to reliably detect loss or gain of one or two hydrogens.

The *meso*-[Ru(dipa)$_2$](PF$_6$)$_2$, *rac*-[Ru(dipa)$_2$](PF$_6$)$_2$, and bromine- and persulfate-oxidized *rac*-[Ru(dipa)$_2$](PF$_6$)$_2$ materials were analyzed by MALDI-TOF mass spectrometry (representative spectra are shown in Figure 8). The mass spectra of *meso*-[Ru(dipa)$_2$](PF$_6$)$_2$ and *rac*-[Ru(dipa)$_2$](PF$_6$)$_2$ each showed only two significant peaks, both of which correspond with singly charged ions. There was no peak for the Ru(dipa)$_2^{2+}$ ion (*m*/*z* 236). The resolution of the spectra ($\Delta m/z = \pm 1$) is insufficient to reliably distinguish between a singly reduced complex [Ru(dipa)$_2^+$] (*m*/*z* 472) and a protonated doubly reduced complex [Ru(dipa)$_2^0$ + H$^+$] (*m*/*z* 473) (hydride addition [Ru(dipa)$_2^{2+}$ + H$^-$] is also a possibility). These two possibilities have been proposed for MALDI mass spectra of polypyridylruthenium(II) complexes.[25] The *m*/*z* 662 peak arises from an adduct of the

(23) Elbergali, A.; Nygren, J.; Kubista, M. *Anal. Chim. Acta* **1999**, *379*, 143−158.
(24) Nakamoto, K. *Infrared and Raman Spectra of Inorganic and Coordination Compounds*; Wiley: New York, 1978.

matrix compound CHCA and the *m*/*z* 473 species. There is no evidence for ion-pair formation with hexafluorophosphate ion.

The mass spectra of the oxidized *rac*-$[Ru(dipa)_2](PF_6)_2$ show four major and a number of less abundant components. The pattern of peaks is not dependent upon the choice of oxidant, bromine or potassium persulfate, though there are some minor variations in the relative intensities of the peaks. The dominant peaks appear at *m*/*z* 442, 458, 474, and 489, indicating the existence of four distinct oxidation products with masses close to that of the parent complex and smaller amounts of heavier compounds (consistent with the chromatographic results described above). The mass spectral data are not sufficiently precise to yield definitive information on the structures of the various products.

Mechanistic Considerations. The mechanism for oxidative dehydrogenation reactions has been the subject of several studies.[26−29] All of these mechanisms begin with a one-electron oxidation of the metal center followed by deprotonation of the amine to yield a highly reactive amidoruthenium(III) intermediate, which then quickly reacts (through several steps) to produce the imine product. The di-2-pyridylmethanamine ligand was chosen for this study, because it contains structural constraints (when coordinated to a ruthenium center) that should prevent creation of a planar bonding geometry at the bridging carbon and thus inhibit imine formation. These constraints, however, should only affect the reactivity of the amidoruthenium(III) intermediate and not reactions leading to formation of that intermediate. This indeed appears to be the case. $Ru(dipa)_2^{2+}$ may be oxidized (chemically or electrochemically) in 1 M H_2SO_4 to $Ru(dipa)_2^{3+}$. Subsequent addition of NaOH to raise the pH leads to rapid formation of the purple oxidation products. Thus, the overall oxidation of $Ru(dipa)_2^{2+}$ follows the expected route of a one-electron oxidation of the metal center followed by amine deprotonation to yield an amidoruthenium(III) intermediate, which rapidly undergoes additional oxidation through as yet unknown steps to yield multiple products.

The effects of the structural restrictions are evident in a comparison of the reactivities of $Ru(bpy)_2(ampy)^{2+}$ and $Ru(dipa)_2^{2+}$. Cyclic voltammetry of the former complex shows irreversible oxidation corresponding with oxidative dehydrogenation of the 2-(aminomethyl)pyridine ligand (ampy) to 2-(iminomethyl)pyridine in 5 M aqueous H_2SO_4.[28a] This behavior is also observed in acetonitrile (a sweep rates below 5 V s^{-1}).[2b,28b] Other Ru(II)-bound primary amines also undergo irreversible oxidation to imines in acetonitrile.[2a] By contrast, $Ru(dipa)_2^{2+}$ shows only a reversible one-electron oxidation in both acetonitrile and strongly acidic aqueous solution, though the half-wave potential for this process in acetonitrile (0.933 V) is somewhat lower than that of $Ru(bpy)_2(ampy)^{2+}$ (1.16 V),[2b] corresponding with a lower driving force for ligand oxidation. At higher pH the $Ru(dipa)_2^{2+}$ complex undergoes irreversible oxidation to yield multiple products, which is reactivity distinctly different from that of the structurally similar $Ru(bpy)_2(ampy)^{2+}$ which reacts to give the 2-(iminomethyl)pyridine complex exclusively.

Conclusions

The spectroscopic and electrochemical properties of $Ru(dipa)_2^{2+}$ (both *rac* and *meso* isomers) are very similar to those of $Ru(bpy)_2(NH_3)_2^{2+}$. MLCT and $\pi \rightarrow \pi^*$ transitions are observed in the visible and UV regions, and solvatochromatic data provide evidence for hydrogen-bond donation by the dipa NH_2 site to the solvent. In strongly acidic aqueous solution, both complexes show a reversible one-electron oxidation: $E_{1/2} = 0.786$ V for $Ru(dipa)_2^{2+}$ (1 M H_2SO_4) and 0.694 V (in 0.1 M CF_3COOH)[30] and 0.66 V in (0.1 M $HClO_4$)[19] for $Ru(bpy)_2(NH_3)_2^{2+}$.

The oxidation of $Ru(dipa)_2^{2+}$ in aqueous solution above pH 3 leads to rapid irreversible transformation of the dipa ligand yielding multiple products. This behavior contrasts sharply with the reactivity of ruthenium(II) complexes of the structurally similar 2-(aminomethyl)pyridine ligand, which undergoes oxidative dehydrogenation to 2-(iminomethyl)pyridine exclusively. The difference in reactivity is attributable to the inability of the $CHNH_2$ carbon in ruthenium-bound dipa to assume the planar (sp^2) geometry required for formation of the imine. One-electron oxidation of $Ru(dipa)_2^{2+}$ to $Ru(dipa)_2^{3+}$ followed by deprotonation yields a highly reactive amidoruthenium(III) intermediate. With the route to imine formation blocked, this intermediate finds other routes for reaction. The nature and products of those routes are the subject of current investigation.

Acknowledgment. The authors thank Marty Faulkner and Brian Cooper for their assistance with the mass spectrometry measurements on the PerSeptive Biosystems instrument at the University of North Carolina at Charlotte. The authors are grateful to Rodger Nutt for helpful discussions.

Supporting Information Available: Figures showing molecular orbital diagrams and isosurfaces. This material is available free of charge via the Internet at http://pubs.acs.org.

IC030242A

(25) (a) Mahn-Jong, K.; Konduri, R.; Ye, H.; MacDonnell, F. M.; Puntoriero, F.; Serroni, S.; Campagna, S.; Holder, T.; Kinsel, G.; Rajeshwar, K. *Inorg. Chem.* **2002**, *41*, 2471−2476. (b) Hunsucker, S. W.; Watson, R. C.; Tissue, B. M. *Rapid Commun. Mass Spectrom.* **2001**, *15*, 1334−1340. (c) Bodige, S.; Torres, A. S.; Maloney, D. J.; Tate, D.; Kinsel, G. R.; Walker, A. K.; MacDonnell, F. M. *J. Am. Chem. Soc.* **1997**, *119*, 10364−10369.

(26) Bernhard, P.; Bull, D. J.; Bürgi, H.-B.; Osvath, P.; Raselli, A.; Sargeson, A. M. *Inorg. Chem.* **1997**, *36*, 2804−2815.

(27) (a) Bernhard, P.; Sargeson, A. M.; Anson, F. C. *Inorg. Chem.* **1988**, *27*, 2754−2760. (b) Bernhard, P.; Sargeson, A. M. *J. Am. Chem. Soc.* **1989**, *111*, 597−606. (c) Bernhard, P.; Anson, F. C. *Inorg. Chem.* **1989**, *28*, 3272−3274.

(28) (a) Ridd, M. J.; Keene, F. R. *J. Am. Chem. Soc.* **1981**, *103*, 5733−5740. (b) Keene, F. R.; Ridd, M. J.; Snow, M. R. *J. Am. Chem. Soc.* **1983**, *105*, 7075−7081.

(29) Toma, H. E.; Tsurumaki, M. *J. Braz. Chem. Soc.* **1990**, *1*, 17−21.

(30) Lai, Y.-K.; Wong, K.-Y. *J. Electroanal. Chem.* **1994**, *374*, 255−261.